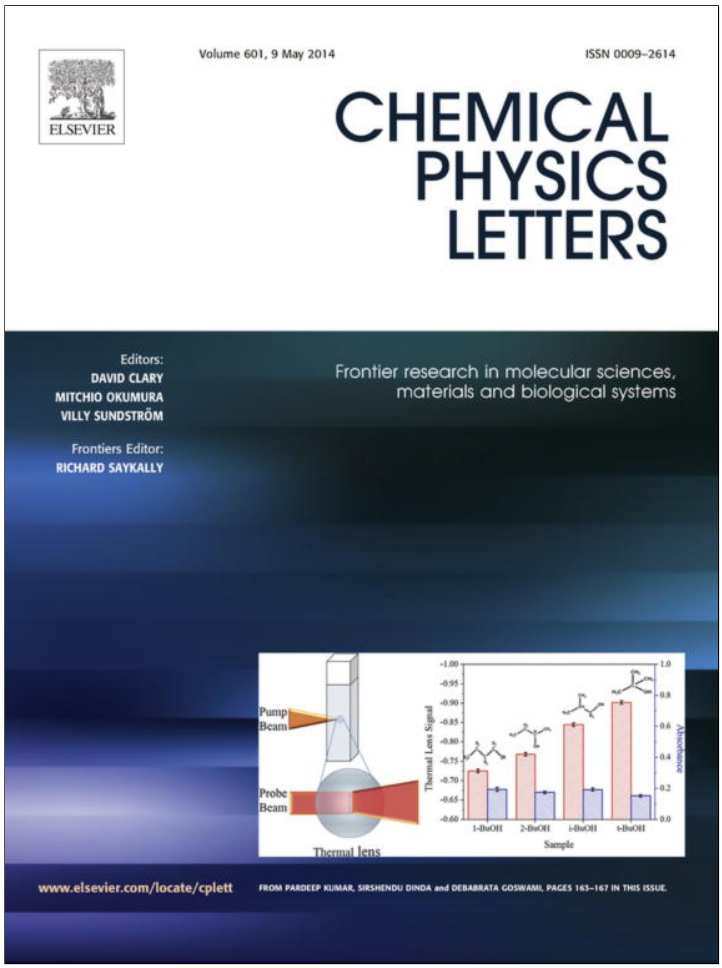

Chemical Physics Letters 601 (2014) 128–133

Contents lists available at ScienceDirect

Chemical Physics Letters

journal homepage: www.elsevier.com/locate/cplett

Optical size effect of organic nanocrystals studied by absorption spectroscopy within an integrating sphere

Yudai Numata [a], Selvakumar V. Nair [b], Kazuya Nakagawa [a], Heisuke Ishino [a], Takayoshi Kobayashi [c], Eiji Tokunaga [a,d,*]

[a] Department of Physics, Faculty of Science, Tokyo University of Science, 1-3 Kagurazaka, Shinjuku-ku, Tokyo 162-8601, Japan
[b] Centre for Advanced Nanotechnology, University of Toronto, 170 College Street, Toronto M5S3E3, Canada
[c] Department of Applied Physics and Chemistry, and Institute for Laser Science, University of Electro-Communications, 1-5-1 Chofugaoka, Chofu, Tokyo 182-8585, Japan
[d] Research Center for Green and Safety Sciences, Tokyo University of Science, 1-3 Kagurazaka, Shinjuku-ku, Tokyo 162-8601, Japan

ARTICLE INFO

Article history:
Received 27 January 2014
In final form 26 March 2014
Available online 4 April 2014

ABSTRACT

The size effect of the optical absorption in one of the most typical organic nanocrystals, α-perylene, was studied. The true absorption spectra of nanocrystals suspended in water were measured within an integrating sphere by collecting the whole scattered light. It was experimentally confirmed that the absorption spectra show blueshift as the crystal size is decreased. This was reproduced by the size-dependent absorption spectra calculated for spherical nanocrystals with isotropic and anisotropic dielectric constants to elucidate three mechanisms of the blueshift: size-dependent change in the shape anisotropy of the crystals, longitudinal–transverse mixing, and light propagation effects including scattering on absorption.

1. Introduction

Organic semiconductors have advantages over inorganic counterparts in production cost, environmental cost, free of scarce elements, flexibility, printability, and practically infinite variety. Recently, organic nanocrystals have also attracted much attention because of their potential for functional nanomaterials [1,2]. In fact, life is made of organic nanomaterials, so that the future of this field is expected to be prosperous.

One of the intriguing issues in this field is the size effect of the optical properties of nanocrystals. For example, perylene nanocrystals of a few hundred nanometers in diameter show an unusual "quantum size effect" with a blue-shifted exciton absorption compared to the bulk crystal [3–8]. Recently, the blue shift was observed to occur for single perylene nanocrystals [9,10] as well as for an ensemble average of nanocrystals. These crystal sizes are more than ten times larger than those of semiconductor quantum dots which show the same amount of blueshift [11]. Similar size-dependent blueshifts are observed also for polymer nanocrystals such as poly-diacetylene nanocrystals [12] and for nanocrystallized charge-transfer complexes such as Cu-TCNQ (tetracyanoquinodimethan) nanocrystals [13], which is also of great interest.

The keys to understanding of the anomalous size effect in organic nanocrystals are their typical size and optical anisotropy. Inorganic semiconductor quantum dots are typically less than 100 nm in size, and their optical anisotropy is relatively small. On the other hand, organic nanocrystals, formed by a self-assembly mechanism such as the reprecipitation method, are 100 nm or more in size, so that the effect of light scattering on the absorption spectra is significant [14]. In both experiment and calculation, we discriminate between extinction and absorption as follows. The extinction spectrum measures the spatial decay of the incident light intensity as a function of the light wavelength due to both absorption and scattering loss. The absorption spectrum describes the decay constant as a function of wavelength only due to the absorption loss, which is measurable when the scattered light over the whole solid angle is collected. Previously the size-dependent absorption spectra of perylene nanocrystals were measured with and without an integrating sphere [15]. As the crystal size is increased from 100 nm, the light scattering causes a redshift in the extinction spectra, resulting in an apparent redshift in the absorption spectra with the size. In addition, it was suggested that the size-dependent crystal shape may affect the absorption spectra due to a large optical anisotropy of the crystal. However, since the

* Corresponding author at: Department of Physics, Faculty of Science, Tokyo University of Science, 1-3 Kagurazaka, Shinjuku-ku, Tokyo 162-8601, Japan. Fax: +81 3 5261 1023.
E-mail address: eiji@rs.kagu.tus.ac.jp (E. Tokunaga).

http://dx.doi.org/10.1016/j.cplett.2014.03.077
0009-2614/

samples were placed in front of the integrating sphere for the absorption measurement, the effect of backward scattering on the spectra was not completely ruled out.

In this Letter, we measured the true absorption spectra of perylene nanocrystals placed inside an integrating sphere. The size-dependent absorption spectra thus obtained are compared with calculated spectra. The calculation includes an accurate model for the dielectric constant (ϵ) of perylene reflecting the crystal and molecular anisotropy as well as electromagnetic propagation effects through numerical scattering calculation using discrete dipole approximation (DDA) [16,17]. Theoretical details are given in the Appendix. Comparison of the experimental spectra with orientationally averaged and the *c*-axis polarized absorption spectra reveals the mechanism of the blue shift.

Since the α-perylene crystal has three distinguishable crystal axes as shown in Figure 1, the exciton structure has a strong crystal orientation dependence as may be seen from Figure 2 [3–7]. The dielectric constant shown in Figure 2 was calculated as described in the Appendix. In bulk crystal, *b*-polarized A_u excitons are usually probed as nearly *c*-polarized B_u excitons are not excited with the light incident on the well-developed *a*–*b* plane. For nanocrystals, on the other hand, other planes may have a more chance to appear such that intense, blue-shifted B_u excitons are more accessible. The energy separation of the two excitons is 67 meV (540 cm^{-1}) [6,10]. The origin of this energy shift may be understood from the nature of the lowest energy exciton state in perylene. It arises from a transition polarized along the long axis of the molecule that splits into two excitonic states with A_u and B_u symmetry in the crystal. The energies of these excitons in our calculated dielectric constant are indicated by the dashed lines in Figure 2. The A_u exciton defines the band-edge and is polarized along the *b*-axis of the crystal. Its oscillator strength is very weak because the *b*-axis nearly orthogonal to the long-axis of the molecule. The B_u exciton is polarized in the $a-c$ plane with a much larger dipole moment as the *c* axis is nearly parallel to the long-axis of the molecule. Thus, in a collection of randomly oriented nanocrystals, the absorption could be dominated by the B_u exciton which is blue-shifted from the A_u exciton by Davydov splitting.

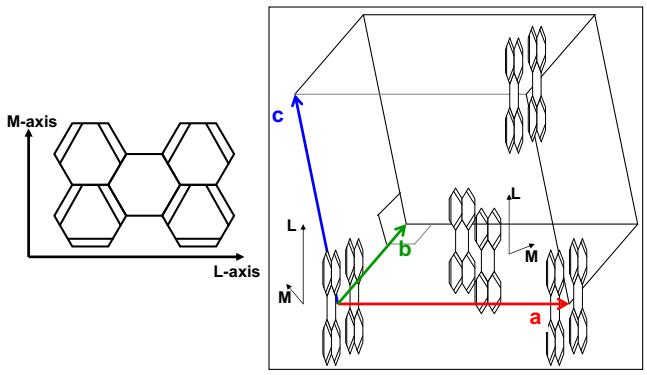

Figure 1. Molecule and α-crystal structure of perylene.

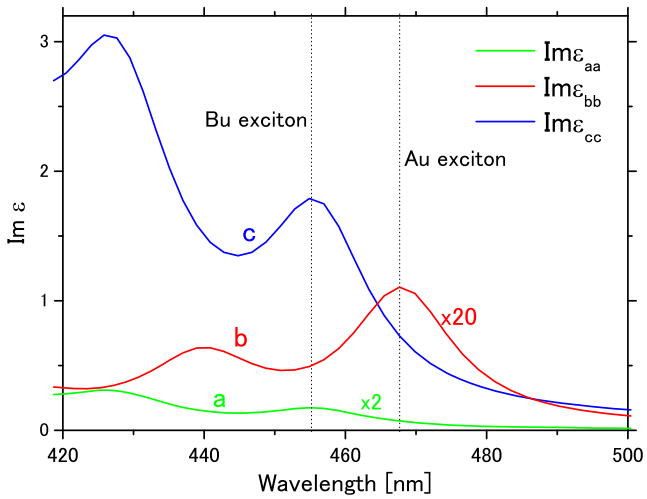

Figure 2. Anisotropic optical spectra of α-perylene crystal, calculated from molecular transition moments as described in the Appendix.

2. Experimental

Perylene nanocrystals were made by the reprecipitation method [18]. Briefly, an aliquot of perylene/acetone solution was mixed with distilled water to crystallize the nanocrystals. Aqueous suspensions of nanocrystals were obtained after vaporizing acetone. Perylene (>98%) (TCI, Tokyo Chemical Industry) was purified once by sublimation. By injecting 200 μL of 1 mM perylene/acetone solution into 5 mL of water once and twice, nanocrystals of average size 136 ± 32 and 230 ± 37 nm were fabricated, respectively. The size was measured with a particle analyzer(FPAR-1000, Otsuka Electronics).

For crystals of diameter larger than 100 nm, the effect of light scattering on absorption measurement is significant in the visible region. To avoid this, the absorbance is usually measured with an integrating sphere in such a way that a sample is placed in contact with the entrance hole of the sphere to collect all the forward-scattered light. In this setup, however, the back-scattered light is counted as the absorbed light. Therefore, to collect the whole scattered light, we made a sample cell locatable inside the sphere to get closer to the true absorption measurement.

Figure 3(a) shows this setup implemented in a commercial integrating sphere in a spectrophotometer (SolidSpec-3700DUV, Shimadzu) for absorbance (Abs.) measurement of the aqueous suspensions of nanocrystals. The sample cell is a custom-made quartz cylinder of 5 mm in height and 3 and 5 mm in inner and outer diameters. The cell was located 15 mm away from the inner wall on the opposite end of the entrance, fixed with a transparent double-sided tape on a transparent glass stage attached to the wall. For comparison, using a 3 mm optical-path-length rectangular cell, we performed the absorbance plus backscattering (Abs.+Back.) measurement with the sample cell in contact with the sphere as

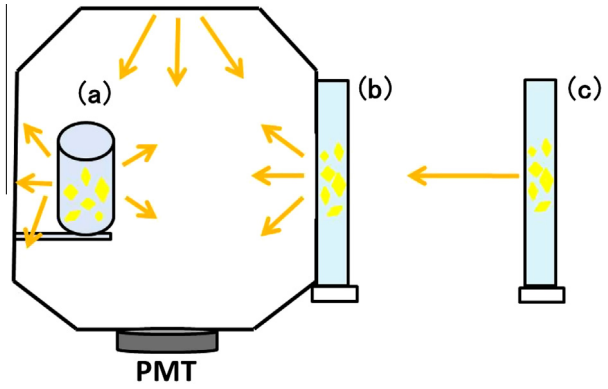

Figure 3. Setup for absorption measurement with an integrating sphere. PMT: photomultiplier tube. (a) Optical loss by absorption (Abs). (b) Optical loss by absorption and backscattering (Abs.+Back.). (c) Optical loss by absorption and scattering (Ext.).

in Figure 3(b) and the extinction (Ext.) measurement with the cell located 10 cm away from the sphere as in Figure 3(c).

3. Results and discussion

Figure 4 shows the absorption, absorption plus backscattering, and extinction spectra of perylene nanocrystals suspended in water for average sizes of 136 nm and 230 nm in diameter. The size distributions of nanocrystals are shown in the inset in Figure 4. The effect of setting the sample inside the sphere is obvious. The signal intensity and lower-energy tail decrease as more scattered light is collected. For 230 nm crystals, the zero-phonon absorption peak in Abs. is blue-shifted from that in Abs.+Back., demonstrating that more accurate absorption spectra are obtained within the sphere.

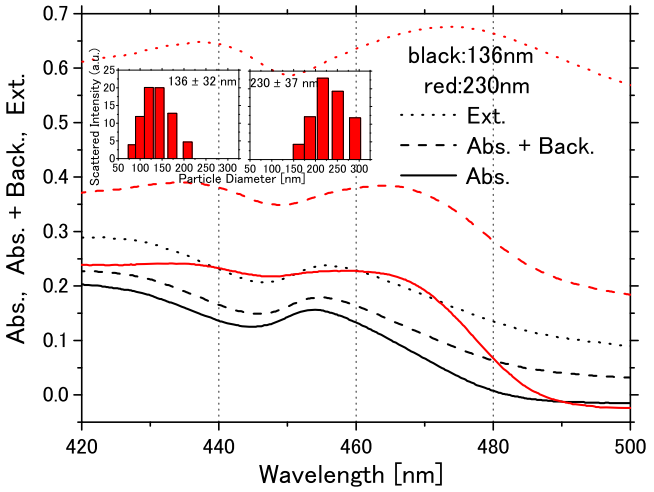

Figure 4. Extinction (dotted lines), absorption plus backscattering (dashed lines), and absorption (solid lines) spectra of aqueous suspensions of perylene nanocrystals of 136 ± 32 nm (black lines) and 230 ± 37 nm (red lines) in diameter. Inset: size distributions of nanocrystals. (For interpretation of the references to colour in this figure legend, the reader is referred to the web version of this article.)

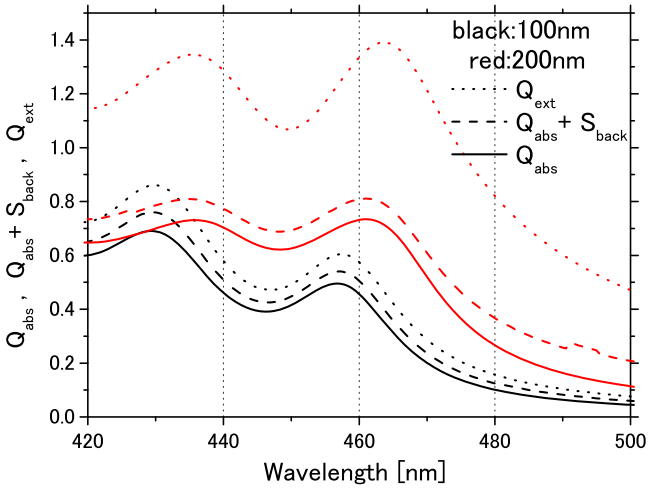

Figure 5. Calculated absorption and scattering spectra of orientationally averaged spherical nanocrystals of 100 nm (black lines) and 200 nm (red lines) in diameter. Q_{ext}: extinction efficiency (solid lines), $Q_{abs} + S_{back}$: absorption plus backscattering efficiency (dashed lines), Q_{abs}: absorption efficiency (dotted lines). (For interpretation of the references to colour in this figure legend, the reader is referred to the web version of this article.)

As the crystal size is increased, the intensity ratio of the one-phonon versus the zero-phonon line is reduced (flattening of the spectra). It is well known that a suspension of absorbing unicellular organisms which contain densely packed pigments exhibit a flattened absorbance spectrum compared with that of a solution containing the same average number density of pigments as homogeneous dispersion; the higher the absorption of the individual cells, the stronger the flattening. This nonlinearity is known as the 'package' effect [14,19], which also can be seen as a reduction in the absorption of pigmented cells relative to the absorption of the same pigments in solution [20]. The observed flattening might be due to a similar effect, but there has been no experimental report about this for organic nanocrystals.

In our previous report [15], the back scattered light is not collected such that there is a possibility that the size-dependent backscattering spectra could affect the size effect on the absorbance. The present measurement finally confirms that the size effect exists for the absorbance of perylene nanocrystals even when the effect of light scattering is completely excluded.

Figure 5 shows results of calculation for the absorption efficiency (Q_{abs}), the absorption and backscattering efficiency ($Q_{abs} + S_{back}$), and the extinction efficiency (Q_{ext}) of spherical perylene nanocrystals 100 nm and 200 nm in diameter with random orientation so that the effect of crystalline anisotropy is averaged. Here back scattering efficiency is calculated by summing all scattered waves with scattering angle greater than 90 degrees. The size dependence of the spectral shape agrees well with the experimental results in Figure 4. In the calculation, the effect of backscattering on the absorbance spectra is very small in remarked contrast to the experiment. This is probably because the experimental spectra contain the contribution of larger crystals than the average in the size distribution. In addition, flattening of the absorption spectra occurs as observed in Figure 4. Because the calculation does not assume an ensemble of nanocrystals but considers single nanocrystals, this is not due to the package effect. One can not tell, therefore, if the experimentally observed flattening of the spectra is caused by the effect of internal scattering on Q_{abs} or due to the effect of molecular aggregation (package effect).

In Figure 6, the experimental absorption spectra of 136 ± 32 nm and 230 ± 37 nm nanocrystals are respectively compared with the calculated spectra of 100 and 150 nm crystals and 200 and 250 nm crystals. In the calculation, two cases of spherical nanocrystals are considered: one is orientationally averaged so that all crystal axes orientations contribute equally, and the other assumes an isotropic ϵ corresponding to the c-axis. Since ϵ along the c-axis is dominated by the contribution of the B_u exciton with a larger oscillator strength and higher energy, the c-axis Q_{abs} is larger than and blue-shifted from the axes-averaged Q_{abs}.

For 136 nm crystals, the energies of the zero and one phonon peaks agree better with those calculated for the c-axis Q_{abs} of 100 nm crystals than those for the axes averaged. This suggests that nanocrystals about 100 nm are dominated by the c-axis Q_{abs}. In addition, the absorption peaks of both calculation and experiment are blue-shifted with respect to that for the imaginary part of ϵ along the c-axis in the bulk. This may be understood in terms of formation of surface modes with mixed longitudinal and transverse character in nanocrystals of size smaller than wavelength as has been extensively studied in semiconductor nanocrystals [21,22]. Energy of the longitudinal field associated with them causes a blue shift compared to the bulk exciton: As the longitudinal (L) exciton has a higher energy than the transverse (T) exciton, the L–T mixed surface mode appears at an intermediate energy between the two and thus at a higher energy than the transverse exciton in the bulk crystal.

For 230 nm crystals, on the other hand, the zero and one phonon peaks are located closer to those calculated for the axes

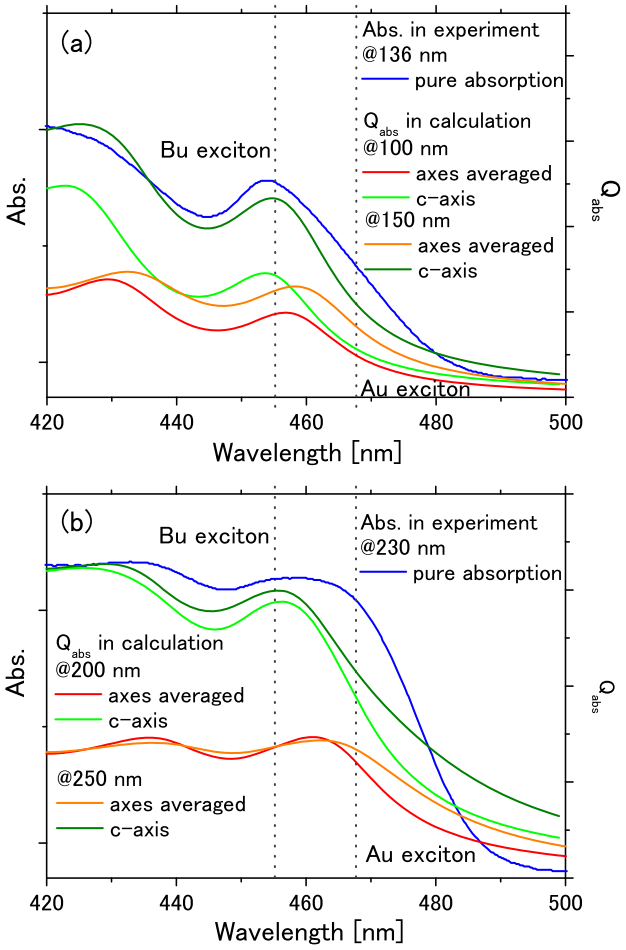

Figure 6. Comparison between the experimental (blue lines) and calculated (light and dark green, red, and orange lines) absorption spectra. The experimental absorption (blue) of 136 ± 32 nm (a) and 230 ± 37 nm (b) crystals is respectively compared with the calculated absorption of 100 (light green and red) and 150 nm (dark green and orange) and 200 (light green and red) and 250 nm (dark green and orange) spherical crystals with the isotropic dielectric constant (ϵ) corresponding to the c-axis (light and dark green) and with the anisotropic ϵ orientationally averaged (red and orange). The dashed vertical lines indicate the A_u and B_u exciton energies in the bulk. (For interpretation of the references to colour in this figure legend, the reader is referred to the web version of this article.)

averaged crystals. These observations strongly suggest the following scenario for the experimental blueshift as depicted by Figure 7: Bulk crystals are platelet crystals with a well developed $a-b$ plane, so that the absorption spectra are dominated by the A_u exciton. As the crystal size is decreased, the crystal shape becomes more cubic for the absorption to reflect the a, b, and c axes' contributions more equally. These shapes are experimentally verified by the images of nanocrystals taken by scanning electron microscopy (SEM) [10,15]. As the crystal size is further reduced to as small as 100 nm, the crystal shape becomes elongated along the c-axis with an $a-c$ or $b-c$ plane dominated. The SEM pictures in Figure 7 support this scenario where pillar shapes are often observed. In the calculation, the blueshift occurs without considering the change in the crystal shape. This is because peaks in absorption are determined by the resonances in ϵ as well as the electromagnetic field profile inside the nanocrystal. The field penetration along the long axis of an elongated nanocrystal will be larger because of smaller depolarization. Thus the calculated results for nanocrystals with the c-axis dielectric constant better describe smaller crystallites that are elongated along the c-axis. Experimentally, the blueshift occurs due to the internal field profile determined by scattering as well as the change in the shape of the crystals.

Three kinds of blue-shifts are summarized as follows: (i) There is the red-shift at large sizes, which appears as blue shift when the size is reduced, caused by internal field enhancement shifting to longer wavelengths due to propagation effects including scattering and multiple reflection (The green curve in Figure 6(b)). (ii) When the size is reduced, the crystal shape and anisotropy is changed (Figure 7). Then, the blue-shift is caused by dominance of the B_u exciton over the A_u exciton due to the large oscillator strength of the former (The red curve in Figure 6(b) to the green curve in Figure 6(a)). (iii) When the size is reduced well below the wavelength, the blue-shift relative to the bulk B_u exciton energy occurs due to longitudinal–transverse (LT) mixing (The green curve in Figure 6(a)).

4. Conclusion

The size effect of perylene nanocrystals on the absorption spectra was evaluated experimentally and theoretically. The true absorption of the samples was measured inside the integrating

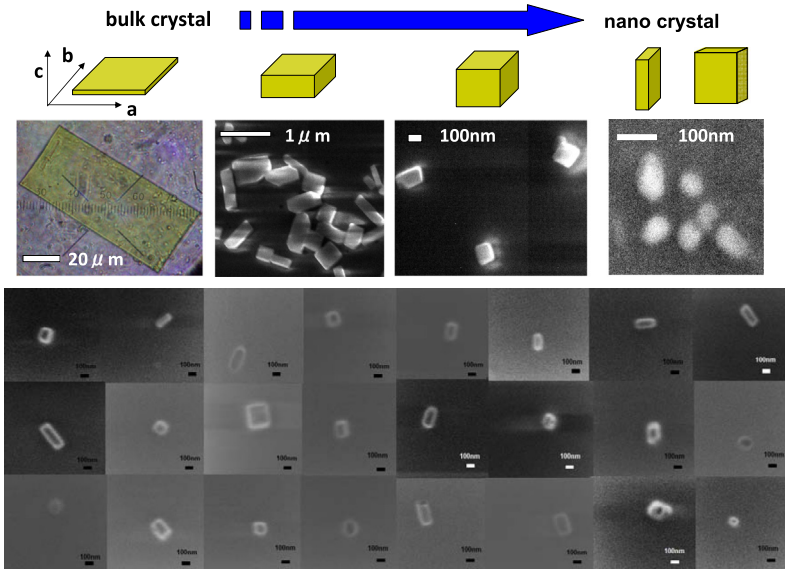

Figure 7. Size-dependent change in crystal shape and scanning electron microscope (SEM) images of nanocrystals with 100 nm scale bars.

sphere by detecting the whole scattered light. It is experimentally verified that the blueshift in the absorbance spectra occurs as the crystal size is decreased. The calculated results agree well with the experimental observations. The mechanism of the size-dependent blueshift is well explained by change in the shape anisotropy of the crystals, LT mixing, and light propagation effects including scattering and multiple reflection on absorption.

Appendix

Electromagnetic scattering from spherical particles of isotropic dielectric constants can be rigorously calculated by the Mie scattering theory [14]. However, perylene is an optically anisotropic crystal of C_{2h} symmetry so that even for spherical shapes a numerical scheme is required for extinction and scattering calculation. We used the discrete dipole approximation (DDA) method [16,17]. The method involves dividing the crystallite of dielectric constant (ϵ) into a discrete cubic array of cells $j = 1, 2 \ldots n$. Each cell is small enough to be described as a point-like dipole with polarizability $\tilde{\alpha}$. We use the Clausius–Mossotti relation to determine $\tilde{\alpha}$ in terms of ϵ

$$\tilde{\alpha} = \frac{3}{4\pi N}[\epsilon - \epsilon_b][\epsilon + 2\epsilon_b]^{-1} \tag{1}$$

where N is the number of lattice points (or dipoles) per unit volume. Note that both ϵ and $\tilde{\alpha}$ are tensors. ϵ_b is the dielectric constant of the background medium which is assumed to be isotropic. The tilde over quantities denote that these are effective properties of the artificial cells into which the crystallite is divided and should not be confused with molecular polarizabilities and dipoles discussed later.

The above procedure reduces the problem to that of scattering by an array of point dipoles which can be handled numerically as follows. The dipole at site $i, \tilde{\mathbf{d}}_i = \tilde{\alpha}\mathbf{E}_i$, where $\mathbf{E}_i$ is the local electric field which is the sum of the field of the incident plane wave $\mathbf{E}_{inc} = \mathbf{E}_0 \exp(i\mathbf{k}\cdot\mathbf{r}_i)$ and the field generated by all other dipoles. Here $\mathbf{r}_i$ is the position of the ith dipole. Using the expression for the field radiated by a point dipole, one gets a set of n simultaneous linear equations

$$\tilde{\mathbf{d}}_i = \tilde{\alpha}\mathbf{E}_0 \exp(i\mathbf{k}\cdot\mathbf{r}_i) + \tilde{\alpha}\sum_{j;\neq i}\frac{\exp(ikr_{ij})}{r_{ij}^3}\left\{k^2(\mathbf{r}_{ij}\times\tilde{\mathbf{d}}_j)\times\mathbf{r}_{ij} + \frac{(1-ikr_{ij})}{r_{ij}^2}\left(3\mathbf{r}_{ij}\mathbf{r}_{ij}\cdot\tilde{\mathbf{d}}_j - r_{ij}^2\tilde{\mathbf{d}}_j\right)\right\} \tag{2}$$

where $k = \sqrt{\epsilon_b}\omega/c, \omega$ being the frequency of the incident field, $\mathbf{r}_{ij} = \mathbf{r}_i - \mathbf{r}_j$.

This system of equations may be efficiently solved using an FFT-based approach. Once the fields and dipoles at each site is self-consistently determined, the extinction cross-section (C_{ext}) and absorption cross-section (C_{abs}) are readily obtained:

$$C_{ext} = \frac{4\pi k}{|E_0|^2}\sum_i \Im(\mathbf{E}_{inc}^* \cdot \tilde{\mathbf{d}}_i) \tag{3}$$

$$C_{abs} = \frac{4\pi k}{|E_0|^2}\sum_i \Im(\mathbf{E}_i^* \cdot \tilde{\mathbf{d}}_i) \tag{4}$$

where $\Im$ denotes the imaginary part. The absorption and extinction efficiencies are defined as the respective cross-section divided by the cross-sectional area of the scatterer [14].

The only input missing for the calculation is the dielectric constant of perylene. While there is little reliable data on the dielectric constant in the visible region of interest, the molecular polarizability α is fairly well-known from solution measurements [3]. Therefore we developed a model for ϵ starting from α and dipole–dipole interaction between the molecules computed using Ewald's method.

Perylene molecule is planar with D_{2h} symmetry and principal axes denoted by L the long-axis, M the short axis and N perpendicular to the plane. Thus α is diagonal with components α_L, α_M and α_N. The crystal has lower symmetry (C_h^5) leading to splitting of the molecular energy levels due to inter-molecular interactions which we treat as dipole–dipole coupling. Inter-molecular interactions that lead to the splitting and energy shifts has a short-range part and a longer range dipole–dipole interaction. The short-range interaction is phenomenologically included as a shift in the spectrum to match with the observed bulk band-gap while the dipole–dipole interaction is accurately included in our model.

Denoting the 4 non-equivalent molecules at lattice site i by $i\mu$ (position $\mathbf{r}_{i\mu}$), with $\mu = 1 \ldots 4$, the local field at site $i\mu$ is given by

$$\mathbf{E}_\mu = \mathbf{E}^0 + \nabla\nabla\sum_{j\nu}{}' \frac{\mathbf{d}_\nu}{|\mathbf{r}_{i\mu} - \mathbf{r}_{j\nu}|} \tag{5}$$

$$= \mathbf{E}^0 + \frac{4\pi}{v_c}\tilde{\mathcal{L}}_{\mu\nu}\mathbf{d}_\nu \tag{6}$$

where $\mathbf{d}_\nu$ is the dipole moment at site ν and v_c is the volume of the unit-cell. The first term is the applied field and the second term is the instantaneous [23] field due to all other dipoles. We have introduced dimensionless dipole sum tensors $\tilde{\mathcal{L}}_{\nu\mu}$ which depend only on the crystal structure. If we represent all molecular dipoles in a local co-ordinate system determined by the L, M, N axes $\tilde{\mathcal{L}}$'s may be expressed in terms of only 4 independent tensors $\mathcal{L}_\mu$ as $\tilde{\mathcal{L}}_{1\mu} = \mathcal{L}_\mu$, $\tilde{\mathcal{L}}_{\mu\nu} = \tilde{\mathcal{L}}_{\mu\nu}$, $\tilde{\mathcal{L}}_{\mu\mu} = \mathcal{L}_1, \tilde{\mathcal{L}}_{23} = \mathcal{L}_4$, and $\tilde{\mathcal{L}}_{24} = \mathcal{L}_3, \tilde{\mathcal{L}}_{34} = \mathcal{L}_2$. Further, by symmetry of the crystal, A_u states have dipole moments along the b-axis and B_u states have dipole moment in the plane perpendicular to the b-axis.

Using these facts and $\mathbf{d}_\nu = \alpha\mathbf{E}_\nu$, we get dipole moment per unit cell, $\mathbf{d}_c$ as

$$\mathbf{d}_c = 4\hat{b}\cdot\left(\alpha^{-1} - \frac{4\pi}{v_c}\mathcal{L}_+\right)^{-1}\mathbf{E}^0\hat{b} + 4\hat{b}\times\left(\alpha^{-1} - \frac{4\pi}{v_c}\mathcal{L}_-\right)^{-1}\mathbf{E}^0\times\hat{b} \tag{7}$$

where $\mathcal{L}_\pm = (\mathcal{L}_1 - \mathcal{L}_2) \pm (\mathcal{L}_3 - \mathcal{L}_4)$. The dipole sum tensors were calculated by Ewald's method [24] for perylene lattice using lattice parameters from Ref. [25]. The results are given in Table 1. From the dipole moment per unit cell ϵ is easily obtained using $\epsilon\mathbf{E}^0 = 1 + 4\pi\mathbf{d}_c/v_c$ and we get,

$$\epsilon_{bb} = \left[1 + 4\left(\frac{v_c}{4\pi}\alpha^{-1} - \mathcal{L}_+\right)^{-1}\right]_{bb} \tag{8}$$

$$\epsilon_{ij} = \left[1 + 4\left(\frac{v_c}{4\pi}\alpha^{-1} - \mathcal{L}_-\right)^{-1}\right]_{ij} \text{ for } i, j \neq b \tag{9}$$

$$\epsilon_{ib} = \epsilon_{bi} = 0 \text{ for } i \neq b \tag{10}$$

where the indices run over the crystal axes a, b and c'.

Thus ϵ is determined if the molecular polarizability α is known. We model the diagonal components of α along the molecular axes as a sum of Lorentzians

Table 1
The dipole sum tensors for perylene crystal in the molecular co-ordinates. The direction cosines of the molecular axes relative to the crystal are [25] $\hat{L} = (0.1173, 0.0138, 0.9930)$, $\hat{M} = (0.5681, 0.8192, -0.0785)$, and $\hat{N} = (-0.8146, 0.5733, 0.0883)$.

state	$\mathcal{L}_{LL}$	$\mathcal{L}_{MM}$	$\mathcal{L}_{NN}$	$\mathcal{L}_{LM}$	$\mathcal{L}_{LN}$	$\mathcal{L}_{MN}$
Ag	1.3961	1.9381	−1.1601	−0.2941	0.9951	−1.6722
Bg	1.5705	−0.2779	−3.4513	−0.6395	1.4329	−1.5919
Au	0.0421	−0.1816	1.9865	0.2579	−0.9128	2.9448
Bu	−1.4463	−0.2377	3.8216	0.5458	−1.3339	0.3706

Table 2
Parameters used in the model for α. For each transition, the transition dipole moment calculated from the oscillator strength are also shown. All data adapted from Ref. [3].

i	ω_i (cm^{-1})	f_i	p_i (Å)	Polarization
1	22 000	0.45	0.79	L
2	23 350	0.30	0.63	L
3	24 800	0.21	0.51	L
4	26 400	0.03	0.19	L
5	39 800	1.32	1.01	M
6	48 500	6.51	2.03	M
7	44 200	0.45	0.56	L

$$\alpha_L(\omega) = \alpha_0 + \frac{e^2}{m}\sum_i \frac{f_i}{\omega_i^2 - (\omega + i\Gamma)^2} \tag{11}$$

with a similar equation for α_L and $\alpha_N = 0$ [26]. The parameters used in the model are given in Table 2.

References

[1] H. Masuhara, H. Nakanishi, K. Sasaki (Eds.), Single Organic Nanoparticles, Springer, Berlin, 2003.
[2] S. Masuo et al., Jpn. J. Appl. Phys. 46 (2007) L268.
[3] J. Tanaka, Bull. Chem. Soc. 36 (1963) 1237.
[4] R.M. Hochstrasser, J. Chem. Phys. 40 (1964) 2559.
[5] J. Tanaka, T. Kishi, M. Tanaka, Bull. Chem. Soc. Jpn. 47 (1974) 2376.
[6] K. Fuke, K. Kaya, T. Kajiwara, S. Nagakura, J. Mol. Spectrosc. 63 (1976) 98. For excitons of mutually orthogonal polarization, refer to Figs. 4 and 5 therein.
[7] A. Matsui, K. Mizuno, M. Iemura, J. Phys. Soc. Jpn. 51 (1982) 1871.
[8] H. Kasai, H. Kamatani, S. Okada, H. Oikawa, H. Matsuda, H. Nakanishi, Jpn. J. Appl. Phys. 35 (1996) L221.
[9] H. Ishino, S. Iwai, S. Iwamoto, T. Okumura, T. Kobayashi, E. Tokunaga, Opt. Rev. 17 (2010) 337.
[10] H. Ishino et al., Phys. Rev. B 84 (2011) 041303(R).
[11] P. Michler (Ed.), Single Semiconductor Quantum Dots, Springer, Berlin, 2009.
[12] J.-A. He et al., J. Phys. Chem. B 103 (1999) 11050.
[13] T. Onodera, S. Matsuo, K. Hiraishi, A. Masuhara, H. Kasai, H. Oikawa, CrystEngComm 14 (2012) 7586.
[14] H.C. van de Hulst, Light Scattering by Small Particles, Dover, New York, 1981.
[15] H. Ishino, S.V. Nair, K. Nakagawa, T. Kobayashi, E. Tokunaga, Appl. Phys. Lett. 99 (2011) 053304.
[16] E.M. Purcell, C. Pennypacker, Astrophys. J. 186 (1973) 705.
[17] B.T. Draine, P.J. Flatau, J. Opt. Soc. Am. A 11 (1994) 1491.
[18] H. Kasai, H. Oikawa, S. Okada, H. Nakanishi, Bull. Chem. Soc. Jpn. 71 (1998) 2597.
[19] A. Morel, A. Bricaud, Deep Sea Res. 28 A (1981) 1375.
[20] J.T.O. Kirk, Light and Photosynthesis in Aquatic Ecosystems, Cambridge University Press, Cambridge, 1983.
[21] H. Ajiki, K. Cho, Phys. Rev. B 62 (2000) 7402.
[22] K. Cho, Optical Response of Nanostructures: Microscopic Nonlocal Theory, Springer, Berlin, 2003.
[23] Retardation gets included in the scattering calculation as may be seen from Eq. 2. Also we do not include the non-analytic contribution in the dipole sum tensors as is appropriate for finding ϵ to be used in the Claussius–Mossotti relation (Eq. 1).
[24] M. Born, K. Huang, Dynamical Theory of Crystal Lattices, Clarendon Press, Oxford, 1954. p. 248.
[25] D.M. Donaldson, J.M. Robertson, J.G. White, Proc. R. Soc. London A 220 (1953) 311.
[26] Low-lying electronic states arise from $\pi - \pi^*$ transitions which are all in-plane polarized so that $\alpha_N = 0$.